Yrast decay schemes from heavy-ion + ^{48}Ca fusion-evaporation reactions. II. $^{59\text{-}60}$Fe and $^{59\text{-}60}$Co†

E. K. Warburton, J. W. Olness, A. M. Nathan, and J. J. Kolata
Brookhaven National Laboratory, Upton, New York 11973

J. B. McGrory*
Oak Ridge National Laboratory, Oak Ridge, Tennessee 37830
(Received 13 June 1977)

Fusion-evaporation reactions induced by beams of 25–55-MeV ^{15}N and ^{18}O on an isotopically enriched ^{48}Ca target have been used to populate high-spin yrast levels in $^{59\text{-}60}$Fe and $^{59\text{-}60}$Co. Measurements consisted of γ-ray excitation functions, angular distributions, γ-γ coincidences, and recoil-distance and Doppler-shift lifetime measurements, from which were deduced the energy levels, γ-ray branching ratios, most probable spin-parity assignments, and level lifetimes. The results of p-γ correlation measurements in the ^{58}Fe$(t, p\gamma)^{60}$Fe reaction are also reported.

[NUCLEAR REACTIONS ^{48}Ca(^{15}N,xn,yp)^{59,60}Fe and $^{59\text{-}60}$Co and ^{48}Ca(^{18}O,$xn,z\alpha$)-^{59,60}Fe. E=25–55 MeV; measured $\sigma(E,E_\gamma)$ and coin; deduced levels; measured $\sigma(E_\gamma,\theta)$; deduced J^π for high-spin levels; measured RDM and DSA; deduced τ_m, $|M(M1)|^2$ and $|M(E2)|^2$, ^{58}Fe$(t,p\gamma)^{60}$Fe; measured p-$\gamma(\theta)$; deduced J^π. Enriched targets, Ge(Li) detectors.]

I. INTRODUCTION

In this second of a series of reports of high-spin yrast decay schemes in nuclei formed by HI + ^{48}Ca fusion-evaporation reactions, we report on ^{59,60}Fe and ^{59,60}Co. These nuclei were formed by the reactions ^{48}Ca(^{15}N, $3np$)^{59}Fe, ^{48}Ca(^{18}O, $3n\alpha$)^{59}Fe, ^{48}Ca(^{15}N, $2np$)^{60}Fe, ^{48}Ca(^{18}O, $2n\alpha$)^{60}Fe, ^{48}Ca(^{15}N, $4n$)^{59}Co, and ^{48}Ca(^{15}N, $3n$)^{60}Co.

The experimental investigations included γ-ray excitation functions and angular distributions, γ-γ coincidence spectra, and lifetime measurements via the Doppler-shift-attenuation method (DSAM) and recoil-distance method (RDM). These procedures, the data-analysis methods, and criteria for establishing decay schemes and spin-parity assignments or preferences have been fully described in the first paper[1] of this series (hereafter referred to as I), to which the reader is referred for a more complete discussion and presentation. In I we described the systematic dependence of ^{11}B + ^{48}Ca fusion-evaporation products on bombarding energy. The yield curves for ^{15}N + ^{48}Ca and ^{18}O + ^{48}Ca have the same general behavior, as is expected since the compound nuclei for ^{11}B, ^{15}N, ^{18}O bombardment of ^{48}Ca ($^{59}_{25}$Mn$_{34}$, $^{63}_{27}$Co$_{36}$, $^{66}_{28}$Ni$_{38}$, respectively) all have the same relative position *vis a vis* the valley of stability. Thus ^{59,60}Co were very strongly formed in ^{15}N + ^{48}Ca at 40-MeV bombarding energy, while ^{59}Fe was formed with medium strength and ^{60}Fe was weakly formed. Also ^{59,60}Fe were formed with weak-to-medium strength in the ^{18}O + ^{48}Ca reaction at 50 MeV.

In the next section we present the decay schemes deduced from these data, and also report on results of p-γ angular correlation studies in the ^{58}Fe$(t, p\gamma)^{60}$Fe reaction. In the final section we discuss our results in the light of shell-model calculations performed in a large-basis configurational space. A composite listing of the γ rays observed in the reactions HI + ^{48}Ca studied to date, prepared in a form similar to that presented in Table II of Ref. 1, is available upon request to one of the authors (E.K.W.).

II. DECAY SCHEMES

A. ^{59}Fe

^{59}Fe was formed via ^{48}Ca(^{15}N, $3np$)^{59}Fe and ^{48}Ca(^{18}O, $3n\alpha$)^{59}Fe. The γ rays associated with the ^{59}Fe decay scheme were identified from the relative intensities observed for their production as a function of both energy and type of projectile. The identification was subsequently confirmed by a comparison between the low-lying level scheme and that established in previous work.[2]

The level scheme deduced from the γ-γ coincidence data and angular distribution measurements is shown in Fig. 1. Only levels observed in the present γ-ray experiments are shown. The states with E_x < 1600 keV can all be identified with previously observed levels[2] and the 2312- and 3560-keV levels may be the same as those observed at

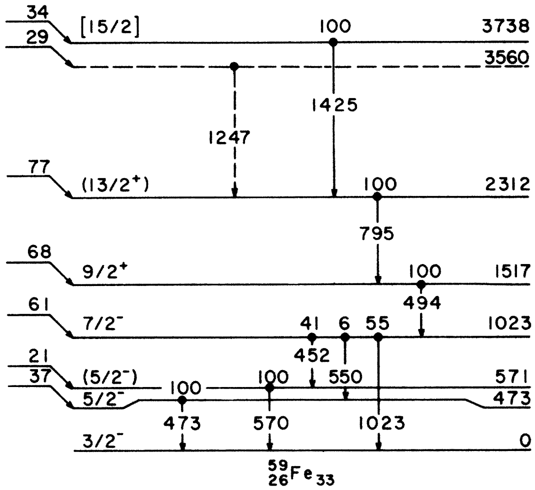

FIG. 1. Placement of ^{59}Fe γ rays observed via $^{48}Ca+{}^{15}N$ and $^{48}Ca+{}^{18}O$ in a level scheme. Except for the 571-keV level all observed levels are assumed to be yrast levels. The spin-parity assignments are discussed in the text. Parentheses enclose assignments not rigorously proved, while the square brackets indicate only a working hypothesis or suggestion. The relative side feeding (arbitrary units) of the levels is indicated on the left. The level at 3560 keV is indicated as uncertain (dashed lines) because the 1247-keV transition could as well originate from a level at 4985.08(84) keV and feed the 3738-keV level. In this case the 4985-keV level would have $J \geq [\frac{15}{2}]$ and the side feeding of the 3738- and 2312-keV levels would be 5 and 106 units, respectively.

2321 ± 10 and 3565 ± 10 keV in the $^{58}Fe(d,p)^{59}Fe$ reaction.[3] None of the γ-ray decay modes shown in Fig. 1 had been reported[2] prior to 1976. However, the decay of the 473- and 571-keV levels was recently observed via $^{59}Mn(\beta)^{59}Fe$.[4] The γ-ray data are collected in Table I which also gives the level energies, branching ratios, relative intensities, and A_2 coefficients from the angular distribution measurements. Note that the γ rays at 1391 and 1790 keV listed in Table I are probably associated with ^{59}Fe but could not be placed in the decay scheme with any certainty.

The mean-life limits listed for the 3560- (or 4985-) and 3738-keV levels are deduced from the DSAM and follow from $F(\tau)$ limits obtained for the 1247- and 1426-keV γ rays (<0.5 and >0.6, respectively). The mean lives of the 2312- and 1517-keV levels were deduced from the RDM assuming a negligible effect of feeding from higher-lying levels. The RDM decay curves for these two transitions are shown in Fig. 2. The lifetimes of the levels below that at 1517 keV could not be determined because of the strong feeding of these levels through the long-lived 1517-keV level.

The spin-parity values assigned to the ground state and 473-keV level are from previous studies.[2] In the $^{58}Fe(d,p)^{59}Fe$ and $^{57}Fe(t,p)^{59}Fe$ work of McLean *et al.*[3] the transitions to low-lying levels of ^{59}Fe were assigned l values in (d,p) and L values in (t,p) as follows: $(E_x, l, L, J^\pi) = (0,1,2,\frac{3}{2}^-)$, $(473,3,2,\frac{5}{2}^-)$, $(571,1,2,\frac{3}{2}^-)$, $(1023,3,4,\frac{7}{2}^-)$, and $(1517,4,5,\frac{9}{2}^+)$, where J^π follows from the identities $\vec{J} = \vec{l} + \frac{1}{2}$, $\vec{J} = \vec{L} + \frac{1}{2}$, and $\pi = (-)^l, \pi = (-)^{L+1}$. The present results are consistent with four of these J^π assignments, but not with $J^\pi = \frac{3}{2}^-$ for the 571-keV level. The direct feeding (see Fig. 1) is stronger than expected for a $\frac{3}{2}^-$ level. Further, the angular distribution of the $571 \to 0$ transition suggests $J+1 \to J$ rather than $J \to J$, while the 452-keV $1023 \to 571$ transition has an angular distribution which is typical of $J+1 \to J$ and completely inconsistent with $J+2 \to J$. Thus, we suggest a probable $\frac{5}{2}^-$ assignment for the 571-keV level. Note that the $l=1$ spectroscopic factor for the 571-keV level was found[3] to be quite small, $(2J+1)S = 0.017$, so that the angular distribution could very well have been influenced by second-order processes. Finally, the J^π assignments to levels above 1600 keV follow from the direct feeding intensities and

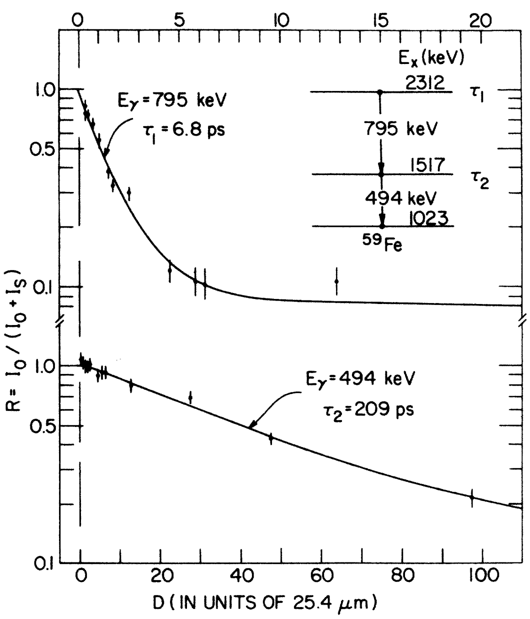

FIG. 2. RDM lifetime results for the ^{59}Fe 795-keV $2312 \to 1517$ transition and 494-keV $1517 \to 1023$ transition. The decay of the intensity of the stopped component I_0 of the transition is plotted as a function of the target-stopper distance D. To first order $D = vt$ where v is the recoil ion velocity, and thus I_0 decays as $\exp(-D/v\tau)$ where τ is the mean life associated with the decay. The least-squares fit given by the solid curves was (to first order) to $A\exp(-D/v\tau) + B$. In the case of the 1517-keV level, due account was taken of the feeding via the 2312-keV level (see insert) by using the relative intensity data of Table I.

TABLE I. γ decay of ^{59}Fe from ^{48}Ca(^{18}O, $3n\alpha$)^{59}Fe and ^{48}Ca(^{15}N, $3np$)^{59}Fe.

E_i [a] (keV)	E_f (keV)	E_γ (keV)	Branching ratio (%)	I_γ [b]	A_2 [b] (%)	$\delta(E2/M1)$ [c]	Mean life [d] (ps)
472.70(10)	0	472.70(10)	100	6101	−25(5)	+0.02(4) or +3.8(6)	...
570.84(13)	0	570.84(13)	100	12761	−56(2)	$-0.15<\delta<-2.1$	...
1023.12(13)	0	1023.09(17)	55±3	14733	9(6)	...	...
	473	550.42(16) [e]	5±2	1523	...	...	...
	571	452.31(11)	40±3	10658	−63(2)	$-0.19<\delta<-2.0$	
1517.21(18)	1023	494.09(13)	100	20821	−29(3)	(0) [f]	209(36)
2312.21(23)	1517	795.00(15)	100	14015	25(3)	(0) [f]	6.8(8)
3559.59(60)	2312	1247.38(55) [g]	100	2856			>0.6
3737.70(64)	2312	1425.47(60)	100	3400	−20(17) [h]	...	<0.4
?	?	1391.48(33)		2096	...		
?	?	1790(2) [i]		...	...		

[a] From the listed γ-ray energies with corrections for nuclear recoil. The γ-ray energies are averages from the two reactions. The numbers in parentheses throughout the table are the uncertainties in the least significant figure.
[b] From ^{48}Ca + ^{18}O at $E(^{18}\mathrm{O}) = 45$ MeV. Intensities in relative units. The A_4 coefficients in the angular distributions were not determined accurately enough to differentiate them from zero.
[c] The $E2/M1$ mixing ratio calculated assuming an alignment parameter, $\alpha_2 = 0.72 \pm 0.15$. The sign convention is that of Rose and Brink (Ref. 5).
[d] The two values with errors are from the RDM, the limits are from the DSAM.
[e] Observed in the γ-γ coincidences only. The listed energy is deduced from the energy level separation.
[f] Assumed to be zero. The A_2 coefficients of the 494- and 795-keV transitions were then used to determine an average alignment parameter α_2.
[g] The 1247-keV γ ray could arise from a 4985.08(84)→ 3737 transition instead of a 3560→ 2312 transition; thus, the 3560-keV level is uncertain.
[h] From ^{48}Ca + ^{15}N.
[i] Observed in the γ-γ coincidences only.

angular distribution measurements.

No evidence was seen in the present studies for the β decay of ^{59}Mn to ^{59}Fe. ^{59}Mn has been observed via ^{13}C + ^{48}Ca both in the present series of measurements and also by Pardo *et al.*[4] Its weaker formation via ^{15}N + ^{48}Ca and ^{18}O + ^{48}Ca is expected since in both cases the exit channels are strongly inhibited in this region of A and Z.

B. ^{60}Fe

The identification of ^{60}Fe γ rays and the placement of these γ rays in a decay scheme was considerably aided by results from an earlier investigation of the ^{58}Fe($t, p\gamma$)^{60}Fe reaction, which had only been reported in abstract form.[6] Nothing further has been reported on the energy levels of ^{60}Fe in the latest Nuclear Data Sheets compilation for $A = 60$.[7] A brief description of the experimental method and resultant conclusions is therefore included at this point.

^{58}Fe($t,p\gamma$)^{60}Fe reaction

Proton-γ ray coincidence spectra from the ^{58}Fe($t, p\gamma$)^{60}Fe reaction were measured using an isotopically enriched (≥82%) target of ^{58}Fe, which was placed at the center of a 12-cm diam chamber and bombarded by 3.0-MeV tritons from the BNL 3.5-MV accelerator. The target for these measurements was prepared by evaporation of a 400-μg/cm^2 layer of ^{58}Fe onto a 0.25-mm tungsten backing. A protective overlay of 400 μg/cm^2 of Au was then evaporated to prevent deterioration of the ^{58}Fe layer when exposed to air. Protons emerging within the angular range $165° \leq \theta_p \leq 174°$ were detected by a 1000-μm annular surface-barrier detector centered at $\theta_p = 180°$ relative to the incident beam direction. A 14-mg/cm^2 Al foil shielded the detector from elastically scattered tritons. Time-coincident γ rays were detected by a Ge(Li) detector, which was positioned on a goniometer so that it could be rotated about the target center. A coincidence circuit with a resolving time of 20 ns was used to gate the two analog-to-digital converters of a TMC 16384-channel analyzer which recorded the p-γ coincidence spectra. For these measurements, 7 digital gates were placed on regions of interest in the proton spectrum (displayed at 1024-channel dispersion), and the coincident γ spectra were stored in associated 2048-channel segments of memory. Due to the presence of light contaminants in the target, separate measurements were performed with carbon and silicon targets in order to clearly establish

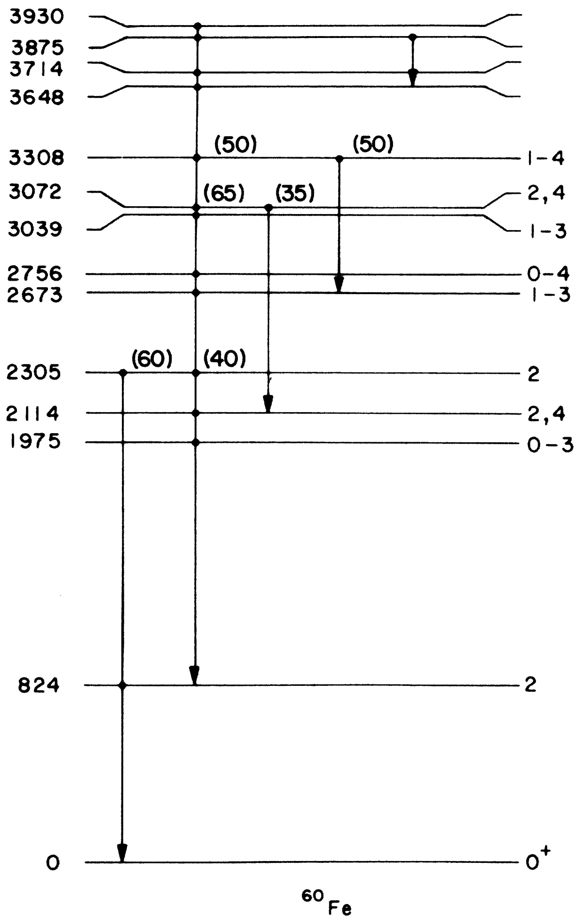

FIG. 3. Level diagram for ^{60}Fe, showing excitation energies, γ-ray branchings, and spin restrictions deduced from the present investigation of the ^{58}Fe$(t,p\gamma)^{60}$Fe reaction at $E_t = 3.0$ MeV. The γ-ray branching ratios are given in parentheses, and have an uncertainty of $\pm$ 10 units.

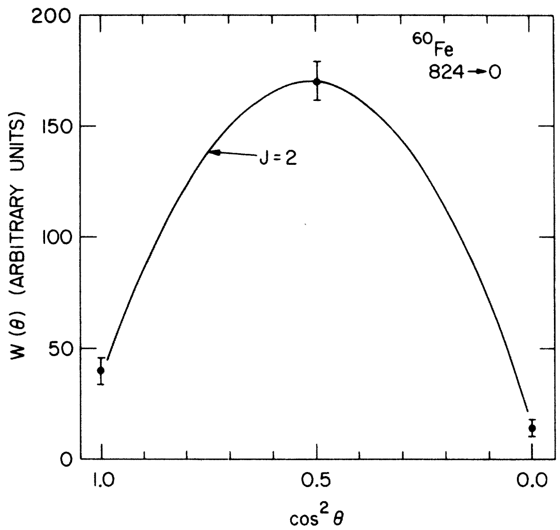

FIG. 4. Angular correlation data for the 824 → 0 transition in ^{60}Fe, resulting from population of the 824-keV level via the ^{58}Fe$(t,p)^{60}$Fe reaction. The solid curve shows the fit to these data for a $J=2$ assignment for the 824-keV level, where the alignment is restricted (as indicated in the text) to magnetic substates $m=0$, ± 1. J = 1 or 3 are excluded by these data.

proton groups belonging to the ^{58}Fe$(t,p)^{60}$Fe reaction. The level scheme for ^{60}Fe deduced from these measurements is shown in Fig. 3.

Measurements were carried out for γ-ray detection angles of $\theta_\gamma = 0°$, 45°, and 90°. The angular correlation information is summarized in Table II, which shows the results of an even-order Legendre-polynomial fit to these data, of the form

$$W(\theta) = I_\gamma[1 + A_2 P_2(\cos\theta) + A_4 P_4(\cos\theta)]. \quad (1)$$

The experimental geometry used in these measurements (i.e., Litherland-Ferguson, method II[8]) insures an alignment of the initial γ-emitting states, and standard techniques of analysis[9] for aligned-correlations were applied to obtain the spin assignments given in Fig. 3. These results will be discussed below for each level in turn.

Because a relatively thick ^{58}Fe target was used in these measurements, the effective resolution for proton detection was inadequate to resolve individual higher-lying states, and in fact the digital gates were ususally set to span clusters of states as indicated in Table II. However, the placement of each gate restricted the range of excitation energy sufficiently well so that the decay scheme could be uniquely constructed from the associated Ge(Li) spectra, which exhibited a resolution of 3–4 keV.

824-keV level. The detection of protons near $\theta_p = 180°$ defines an alignment of the initial γ-emitting state, with the magnetic quantum number (m)—specifying the spin projection—restricted to $m=0$ or ± 1, where the axis of quantization is the beam axis.[8] A small population of higher substates is allowed by the finite size of the proton detector and was taken into account in fitting the correlation patterns. For the 824-keV level, the alignment results in a very strong correlation pattern as shown in Fig. 4. The spin of the ^{60}Fe ground state is $J_f = 0$, and therefore the ground-state transition from the 824-keV level (of spin J) is restricted to be a pure multipole of order $L=J$. The solid curve in Fig. 4 shows an excellent fit for $J=2$, while the corresponding fits for $J=1$ and 3 eliminate these possibilities at the 99.9% confidence level.

1975- and 2114-keV levels. Both levels decay to the 824-keV level. Since the particle groups were unresolved by the proton detector, the correlation pattern for the resultant 824 → 0 transi-

TABLE II. Results of p-γ angular correlation measurements in the ^{58}Fe$(t,p\gamma)^{60}$Fe reaction at $E_t = 3.0$ MeV. The initial states (E_x) falling within specific gates set on the proton spectra are indicated, while subsequent cascade transitions resulting from deexcitation of that state are labeled by giving the energies of the initial and final states between which the transition occurs.

Gate no.	E_x [a] (keV)	$E_i \rightarrow E_f$ (keV)	I_γ	Angular distribution [b] A_2 (%)	A_4 (%)
1	824	824 → 0	439 ± 33	71(4)	−131(5)
2	1975	1975 → 824	270 ± 10	−3(11)	−11(13)
	2114	2114 → 824	73 ± 21	129(41)	−58(34)
3	2305	2305 → 0	342 ± 47	62(6)	−158(10)
		2305 → 824	246 ± 33	17(12)	−33(14)
		824 → 0	441 ± 32	6(7)	−5(8)
4	2673	2673 → 824	1709 ± 81	39(5)	−3(6)
	2756	2756 → 824	139 ± 42	−6(29)	−8(34)
5	3039	3039 → 824	900 ± 66	21(8)	−10(9)
	3072	3072 → 824	537 ± 56	36(10)	−34(11)
		3072 → 2114	315 ± 45	70(12)	−61(14)
		2114 → 824	376 ± 48	46(12)	−47(13)
	3308	3308 → 824	317 ± 44	33(14)	−17(16)
		3308 → 2673	290 ± 35	−28(12)	20(13)
		2673 → 824	446 ± 62	70(13)	3(17)

[a] The uncertainties in the quoted excitation energies increase approximately linearly, from ±1 keV for the 824-keV state to ±3 keV for the 3308-keV state.

[b] The statistical uncertainties in the least significant figure are given in parentheses.

tion involves feeding from both levels and hence was not analyzed. The 1975 → 824 correlation is isotropic within experimental uncertainty, which would be expected for $J(1975) = 0$. These data can also be fitted for spin possibilities $1 \leq J \leq 3$ with large quadrupole/dipole mixing in the 1975 → 824 transition. The 2114 → 824 transition exhibits a nonzero A_4 coefficient, which is confirmed by the pattern observed in the deexcitation of the 3072-keV level (see Table II). This observation restricts the spin of the 2114-keV level to $J \geq 2$. Analysis of the net data on the 2114 → 824 transition, resulting both from direct population of the 2114-keV level and also via the 3072 → 2114 cascade transition, eliminates the possibilities $J = 3$ or 5. Thus one is left with the conclusion $J = 2$ or 4, as given in Fig. 3.

2305-keV level. The results of a simultaneous fit to the net correlation data on the 2305-keV level is shown in Fig. 5. The lower figure shows the "goodness-of-fit" parameter χ^2 plotted as a function of x, the $(L+1)/L$ multipole mixing in the 2305 → 824 transition. The 2305 → 0 transition is, of course, a pure multipole, with $L = J \neq 0$. Satisfactory fits are obtained for $J = 2$ with mixing ratios $x = -(4.3^{+1.5}_{-3.8})$ and $x = +(0.27^{+0.13}_{-0.11})$. For comparison, the best fits for $J = 1$ or 3 exceed the 0.1% confidence limit for all values of x. The upper curve of Fig. 5 shows the calculated fit to the experimental correlation data for parameters corresponding to the χ^2 minimum of the lower plot ($x = -4.3$).

Levels at $E_x > 2600$ keV. For most of these cases, the ambiguities inherent in the analysis of correlation patterns for transitions deexciting to states of $J_f \geq 2$ result in spin limits rather than spin assignments for the initial states. Thus for the 2673-, 2756-, and 3039-keV states one obtains the range of allowed J values indicated in Fig. 3. For the 3072-keV level, however, a simultaneous fit to the 3072 → 824 and 3072 → 2114 → 824 transitions results in the restriction to $J = 2$ or 4. If $J = 4$, the 3072 → 824 transition is pure quadrupole while the 3072 → 2114 transition must involve a significant quadrupole admixture. For the $J = 2$ possibility, both transitions must involve large quadrupole/dipole mixings. Although three cascade transitions were identified for the 3308-keV level, the relatively larger uncertainties in the A_2 and A_4 coefficients results in a weak restriction on the spin of this state. For levels of $E_x > 3600$ keV, the quality of the angular-correlation data did not even admit of significant restrictions on the spins of the states.

^{48}Ca(^{15}N,2np)^{60}Fe and ^{48}Ca(^{18}O,2nα)^{60}Fe

^{60}Fe was formed by the ^{48}Ca(^{15}N, $2np$)^{60}Fe and ^{48}Ca(^{18}O, $2n\alpha$)^{60}Fe reactions. The 2114 → 824 → 0 cascade, known from the ^{58}Fe$(t,p\gamma)$ studies dis-

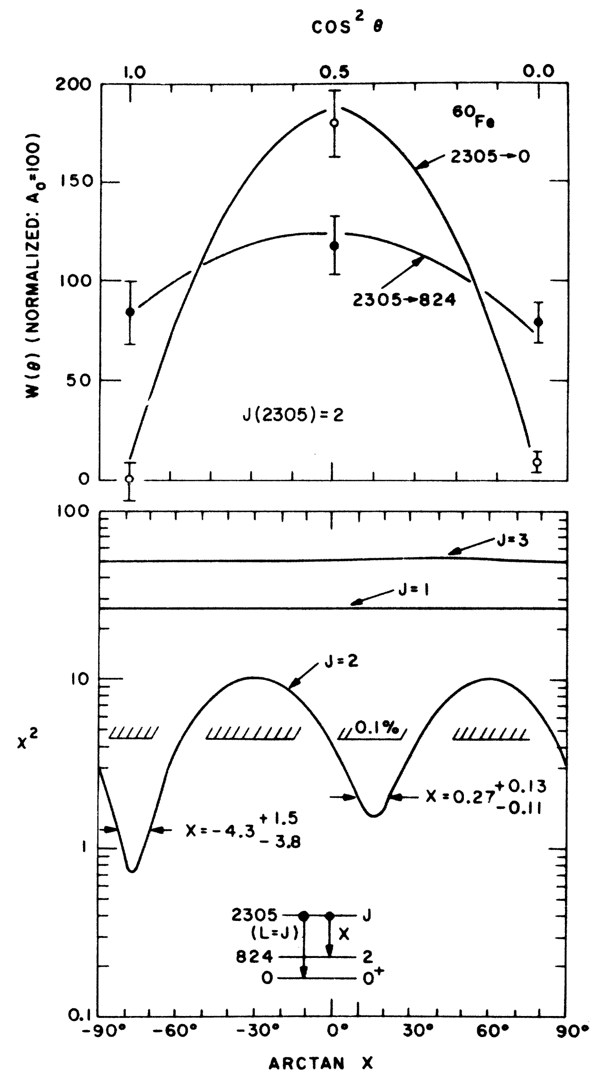

FIG. 5. Results of angular correlation measurements for the ^{60}Fe 2305-keV level, as observed via the ^{58}Fe$(t,p\gamma)^{60}$Fe reaction. The upper plot shows the measured correlation data, while the lower plot illustrates the results of fits to these data for assumed spins for the 2305-keV level of $1 \le J \le 3$. Only for $J=2$ is the fit acceptable, for the allowed quadrupole/dipole mixings indicated. The correlations calculated for these cases are shown in the upper plot by the solid curves.

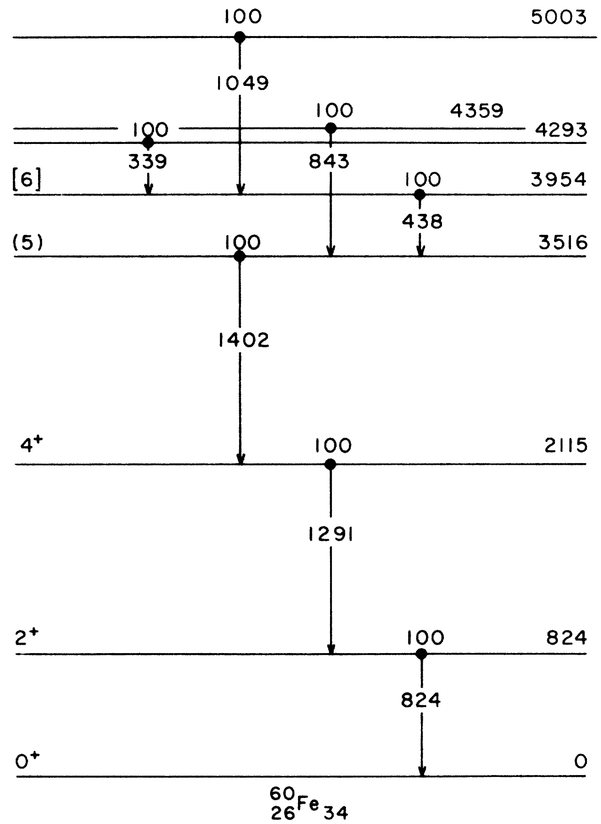

FIG. 6. Level scheme deduced from ^{60}Fe γ rays observed via the ^{48}Ca + ^{15}N and ^{48}Ca + ^{18}O reactions. The levels above 2.5-MeV excitation had not been previously observed. The spin-parity assignments for the 824- and 2115-keV levels are from the (t,p) results and the fusion-evaporation results as discussed in the text.

cussed above, provided the basis for the identification of ^{60}Fe and the γ rays from both reactions as determined from the γ-γ coincidence data are listed in Table III. Because of difficulties due to unresolved contaminants from other nuclei, the analysis of the γ-ray singles data was unusually difficult, and it was necessary to incorporate data from both reactions in order to determine the cascade ordering of the γ-ray transitions. The relative intensities of the γ rays observed in the two reactions were assumed to be proportional, and the data of Table III were combined to give the adopted energies, intensities, and angular distributions listed in Table IV. The level scheme deduced from these results is shown in Fig. 6.

Information relating to the lifetimes of the levels is also collected in Table IV. The DSAM lifetime for the 5003-keV level, and two other lifetime limits, result from the $F(\tau)$ attenuation factors obtained in ^{48}Ca + ^{15}N (Table III). RDM results for the 1291- and 824-keV transitions are shown in Fig. 7. In both RDM decay curves, a long-lived component $\tau = 70 \pm 30$ ps was present. It is assumed that this lifetime is associated with the 3516-keV level; however, it is also possible that it is due to one or more of the levels feeding the 3516-keV level. The mean lives found for the 824- and 2115-keV levels correspond to $E2$ strengths of 13.0 ± 2.0 and 13.3 ± 3.0 W.u. (Weisskopf units), respectively.[10] Since the corresponding $M2$ strengths would be larger by a factor of 50, $M2$ is excluded[10] and so, in agreement with the (t,p) data (Fig. 3), we have $J^{\pi} = 2^+$ for the 824-keV

TABLE III. γ-ray transitions observed in ^{48}Ca + ^{15}N and ^{48}Ca + ^{18}O and assigned to ^{60}Fe.

^{48}Ca + ^{15}N					^{48}Ca + ^{18}O				
E_γ (keV)	Intensity [a]	A_2 [b] (%)	Contaminant [c]	$F(\tau)$ [d]	E_γ (keV)	Intensity [a]	A_2 [b] (%)	Contaminant [c]	$F(\tau)$ [d]
338.61(12)	2 028	···	···		338.61(12)	2 324	···	···	<0.5
438.24(30)	~3 000	···	^{23}Na		438.28(13)	4 473	−5(8)	···	<0.5
824.00 [e]	21 600	···	^{60}Co	···	823.63(15)	21 600	14(2)	···	
843.32(17)	<4 937	···	^{27}Al	···	842.17(16)	<6 243	17(12)	^{62}Ni	
1048.57(12)	2 243	13(15)	···	0.30(15)	1048.00 [e]	<8 600	···	*U*	
1291.00 [e]	<20 618	18(2)	^{59}Co	<0.10	1290.88(18)	19 628	18(2)	···	
1401.56(19)	7 270	−25(5)	···	<0.25	1402.00 [e]	<8 500	···	^{62}Ni	

[a] Arbitrary units. The intensities for the two different target-projectile combinations are normalized so that the intensities of the 824-keV γ ray are equal.
[b] The γ-ray angular distribution is given by $W(\theta) = I_\gamma[1 + A_2P_2(\cos\theta) + A_4P_4(\cos\theta)]$. The A_4 coefficients were not determined with sufficient accuracy to distinguish them from zero.
[c] γ rays assigned to the listed nuclei were unresolved from the ^{60}Fe γ rays. For the 438- and 824-keV γ rays from ^{15}N + ^{48}Ca it was possible to estimate the relative intensities of the unresolved doublets; for the other cases only upper limits on the ^{60}Fe intensities can be given. *U* denotes a γ ray of unknown origin.
[d] The DSAM attenuation factor defined in the text.
[e] Nominal energy.

level and $J^\pi = (2,4)^+$ for the 2115-keV level. For the latter we choose $J^\pi = 4^+$ as highly likely because it is the state with the largest direct feeding. The angular distributions (Table IV) and direct feeding intensities also lead to the spin suggestions given in Fig. 6 for the 3516- and 3954-keV levels.

C. ^{59}Co

The nucleus ^{59}Co was formed via ^{48}Ca(^{15}N, $4n$)^{59}Co. The results are presented in Table V and Fig. 8. The β decay of ^{59}Fe to ^{59}Co was observed to populate several low-spin levels in addition to those shown in Fig. 8. However, this β decay is well known[2] so that only the yrast levels formed via (^{15}N, $4n$) are shown. The levels at 1191 and 1460 keV have previously[2] been given the spin-parity assignments shown in Fig. 8. No previous information exists concerning the γ-decay or spin-parity assignments of the remaining levels. The spin-parity assignments shown in Fig. 8 follow from the arguments outlined in I based on γ-ray relative intensities, angular distributions, and mean lives.

A previous study of ^{59}Co via the ^{62}Ni(p, α)^{59}Co reaction by Mateja *et al.*[11] has been carried out with exceptionally good energy resolution ($\Delta E \sim 1-3$ keV) so that a correlation between the levels observed in (p, α) and (^{15}N, $4n$) can be made with very high accuracy. In the (p, α) work 107 levels were reported below 4.8-MeV excitation energy and, as indicated in Table V, 9 (or possibly 10) of these can be identified with levels we deduce to lie in this energy region. Correspondingly, the ^{59}Co levels of Fig. 8 and Table V not reported by Mateja *et al.* are all assigned $J \geq \frac{15}{2}$ in our work, which presumably explains why they are not populated in the (p, α) reaction.

TABLE IV. γ decay of energy levels of ^{60}Fe from ^{48}Ca(^{15}N, $2np$)^{60}Fe and ^{48}Ca(^{18}O, $2n\alpha$)^{60}Fe.

E_i [a] (keV)	E_f (keV)	E_γ [b] (keV)	Intensity [c]	A_2 [c] (%)	τ [d] (ps)
823.64(15)	0	823.63(15)	21 600	14(2)	11.6 ± 2.2 [e]
2114.52(23)	824	1290.88(18)	19 268	18(2)	1.2 ± 0.3 [e]
3516.10(30)	2115	1401.56(19)	7 270	−25(5)	70 ± 30 [e]
3954.38(33)	3516	438.28(13)	4 400	−5(8)	>0.6
4292.99(35)	3954	338.61(12)	2 176	···	>0.6
4359.11(58)	3516	843.00(50)	<5 000	···	···
5002.96(35)	3954	1048.57(12)	2 243	13(15)	$1.2^{+1.8}_{-0.5}$

[a] Corrected for nuclear recoil. From the γ-ray energies of column 3.
[b] Uncorrected for nuclear recoil. From Table III.
[c] From Table III.
[d] From the DSAM (see Table III) unless otherwise noted.
[e] From the RDM.

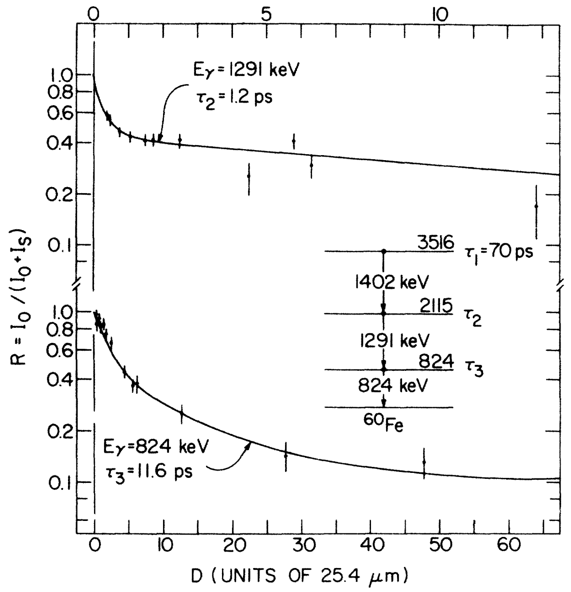

FIG. 7. RDM lifetime results for the ^{60}Fe 1291-keV 2115→824 and 824-keV 824→0 transitions. The decay of the intensity of the stopped component I_0 of the transition is plotted as a function of the target-stopper distance D. To first order $D=vt$ where v is the recoil ion velocity, and thus I_0 decays as $\exp(-D/v\tau)$ where τ is the mean life associated with the decay. The least-squares fit given by the solid curves was (to first order) $A[f_i \exp(-D/v\tau_1)+(1-f_i)\exp(-D/v\tau_i)]+B$ where $i=2$ (upper curve) or 3 (lower curve). In these cases f_i expresses the relative feeding fraction for cascade feeding via observed slow transitions, as opposed to feeding via transitions of negligible lifetime. The values obtained from these fits for the f_i agreed with the relative γ-ray intensities of Table IV.

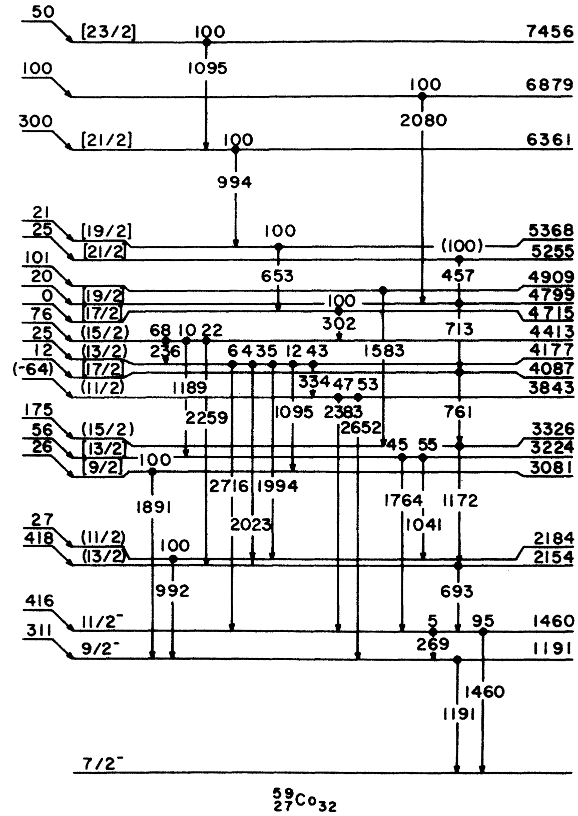

FIG. 8. Level scheme for ^{59}Co deduced from observation of γ rays from the ^{48}Ca(^{15}N, $4n$)^{60}Co reaction. The notation is similar to that of Figs. 1 and 6. Only the yrast (or near-yrast) levels observed in the present studies are shown. Data on the γ-ray transitions are given in Table V.

The process of deducing a decay scheme for ^{59}Co from the γ-γ coincidence data was hampered by the large number of energy degeneracies. The pairs 691 keV(^{60}Co)-693 keV(^{59}Co) and 333 keV(^{60}Co)-334 keV(^{59}Co) were particularly troublesome since these γ rays are important to both decay schemes. The separation between ^{59}Co and ^{60}Co was aided by a survey run for ^{14}N + ^{48}Ca at $E(^{14}\mathrm{N})=45$ MeV which produced ^{59}Co strongly from ^{48}Ca(^{14}N, $3n$)^{59}Co but only negligible ^{60}Co from ^{48}Ca(^{14}N, $2n$)^{60}Co. Also troublesome were the 992-994- and 1095-1096-keV doublets in ^{59}Co which were untangled using the γ-γ coincidence data and the difference in Doppler shifts of the γ rays to deduce γ-ray energies and relative intensities.

The decay scheme of Fig. 8 has one outstanding discrepancy which remains to be explained. Namely, the feeding into the 3843-keV level is considerably greater than the intensity depopulating it. (Thus, the negative direct feeding indicated for this level in Fig. 8.) We assume that one or more transitions depopulating this level have been overlooked. For instance, a ground-state transition would be detected with decreased efficiency (by virtue of its high energy). A study via ^{62}Ni(p, $\alpha\gamma$)^{59}Co would be very helpful here.

The RDM data for ^{15}N + ^{48}Ca was inferior to that for ^{18}O + ^{48}Ca in that the distance of closest approach was ~30 μm as compared to ~10 μm. Thus, the RDM measurements for ^{15}N + ^{48}Ca were insensitive to mean lives $\tau \lesssim 6$ ps, as opposed to the lower limit $\tau \lesssim 2$ ps for ^{18}O + ^{48}Ca. Furthermore, the DSAM results indicate that the majority (and perhaps all) of the observed transitions are quite fast ($\tau \lesssim 1$ ps). Thus no RDM lifetimes were obtained. DSAM lifetimes and limits are listed in Table V.

D. ^{60}Co

^{60}Co was observed via ^{48}Ca(^{15}N, $3n$)^{60}Co. The decay scheme deduced from the data summarized in Table VI, is shown in Fig. 9. All known[7] levels with $E_x < 600$ keV are shown, and their spin-parity assignments, save that for the 436-keV level, are

TABLE V. γ decay of ^{59}Co from ^{48}Ca(^{15}N, $4n$)^{59}Co.

E_i [a] (keV)	E_f (keV)	E_γ [b] (keV)	Branching ratio [c]	I_γ [d]	A_2 [e] (%)	$F(\tau)$ [f]	τ [g] (ps)	$E_i(p,\alpha)$ [h] (keV)
1190.63(28)	0	1190.62(P) [i]	100	68 800	−25(67)	0.37(2)	...	1191.4(9)
1459.64(26)	0	1459.62(26)	95 ± 1	129 136	23(1)	0.17(2)	...	1459.3(9)
	1191	260.01(11)	5 ± 1	7 228	−41(3)	...	...	
2153.58(33)	1460	693.94(20) [j]	100	85 000	...	...	...	2153.6(10)
2183.22(32)	1191	992.88(12)	100	19 696	−15(2)	...	...	2183.5(10)
3081.46(57)	1191	1890.80(50)	100	6 719	43(16)	0.47(4)	<0.6	3082.3(12)
3224.01(30)	1460	1764.22(23)	45 ± 3	4 598	−6(8)	<0.30	<1.0	3222.6(11)
	2183	1040.84(18)	55 ± 3	5 536	3(6)			
3325.72(39)	2154	1172.13(20)	100	33 241		0.79(5)	0.16(30)	
3842.77(32)	1191	2651.60(50)	53 ± 5	4 063	<0	<0.20	...	3842.8(15)
	1460	2383.30(28)	47 ± 6	1 836	41(17)			
4086.54(41)	3326	760.81(13)	100	5 686	−59(8)	>0.5	<0.6	(4088.0(2.7))
4176.80(38)	1460	2716.37(50)	6 ± 2	1 836	...	<0.20	...	4177.9(28)
	2154	2023.22(P)	4 ± 2	1 270	...			
	2183	1993.60(23)	35 ± 5	11 449	−34(3)			
	3081	1095.57(18)	12 ± 3	4 096	−30(10)			
	3843	333.89(30) [j]	43 ± 10	14 000	<0			
4412.70(38)	2154	2259.28(25)	22 ± 4	9 988	−33(2)	<0.20	...	
	3224	1188.69(P)	10 ± 3	4 500	...			
	4177	235.72(11)	68 ± 5	30 170	−30(1)			
4715.05(48)	4413	302.35(30)	100	(37 072)	<0	33(10)	1.1(4)	4715.0(15)
4798.78(50)	4087	712.23(30)	100	4 468	−33(8)	1.00(10)	<0.20	
4909.05(50)	3326	1583.31(31)	100	10 089	49(6)	0.91(5)	0.11(5)	
5256.30(88)	4799	457.50(73)	100	2 493	−21(33)	...	...	
5368.05(49)	4715	653.00(10)	100	37 072	−28(1)	0.92(5)	0.10(5)	
6362.19(57)	5368	994.13(30)	100	35 000	...	>0.80	<0.20	
6878.84(78)	4799	2080.02(60)	100	10 024	...	>0.90	<0.15	
7457.3(11)	6362	1095.08(90)	100	5 000	−30(10)	>0.90	<0.15	

[a] Corrected for nuclear recoil. Uncertainties in the least significant figure are in parentheses.
[b] An entry of P for the uncertainty indicates that the energy was not measured and the quoted E_γ is determined by the level separations.
[c] The numbers in parentheses are from the literature (Ref. 2).
[d] The relative γ-ray intensity. Values in parentheses are estimated.
[e] The γ-ray angular distribution is given by $W(\theta) = I_\gamma[1 + A_2 P_2(\cos\theta) + A_4 P_4(\cos\theta)]$. The A_4 coefficients were not determined with sufficient accuracy to distinguish them from zero.
[f] The DSAM attenuation factor defined in the text.
[g] The mean life of the level (E_i) extracted from $F(\tau)$.
[h] From Ref. 11.
[i] From Ref. 2.
[j] Unresolved in singles spectra from γ rays assigned to ^{60}Co. The data were obtained from the coincidence data and by using the ^{48}Ca(^{14}N, $3n$)^{59}Co reaction since ^{60}Co is formed very weakly via ^{14}N + ^{48}Ca.

from previous[7] work. For this level we choose 5^+ from the $3^+, 4^+, 5^+$ alternatives, because as discussed below, we assign $J = 6$ to the 1216-keV level and observe dipole character for the 780-keV 1216 → 436 transition. The spin-parity of the 786-keV level is also known from previous[7] work. The γ-ray branching ratios for the levels of Fig. 9 with $E_x < 800$ keV are either from previous work or consistent with it (see Table VI). The present observations are consistent with all previous spin-parity assignments for $E_x < 800$ keV.

As shown in Fig. 9, the levels observed with $E_x < 1$ MeV all have $J \leq J_{g.s.}$. Thus it is not surprising that the bulk of the ^{48}Ca(^{15}N, $3n$)^{60}Co cross section is into excited states with $E_x > 1$ MeV. None of the γ decays of these levels have been observed previously. Because the 1216-keV level has one of the largest relative direct feeding cross sections, it is assumed to be an yrast level, i.e., $J \geq 6$. The mean life then is fast enough[10] to insure that the 1216 → 436 transition is at least partially dipole, and so the 1216-keV level has $J = 6$ since the 436-keV state has[7] $J^\pi = 3^+, 4^+, 5^+$. Then, $J^\pi = 5^+$ can be chosen for the 436-keV level. In the ^{59}Co(d, p)^{60}Co angular distribution measurements of Enge, Jarrell, and Angelman[12] a doublet was observed with the more intense member at 1207 ± 6 keV assigned a probable $l = 1 + 3$ transfer. This

TABLE VI. γ decay of ^{60}Co from ^{48}Ca(^{15}N, $3n$)^{60}Co.

E_i [a] (keV)	E_f (keV)	E_γ [b] (keV)	Branching ratio [c] (%)	I_γ [d]	A_2 [e] (%)	$F(\tau)$ [f]	τ [g] (ps)
58.603(7)	0	58.60(P)[h]	100	···	···	···	
277.02(11)	0	277.02(11)	100	12 549	−17(1)	···	
288.43(11)	59	229.83(11)	100	3 051	−19(8)	···	
435.62(16)	0	435.62(P)	(17)	(2 710)	···	···	
	277	158.60(11)	(83)	13 233	−14(4)	···	
506.15(24)	59	447.55(24)	100	1 693	−60(38)	···	
542.56(17)	59	483.96(P)	(22)	(108)	···	···	
	288	254.13(13)	(78)	384	···	···	
785.67(50)	0	785.67(P)	(46)	(1 210)	···	>0.10	<4.5
	288	497.14(52)	(54)	1 421	···	···	
1216.00(20)	0	1216.14(20)	74 ± 5	26 883	<0	0.47(10)	$0.4^{+0.3}_{-0.2}$
	436	779.91(16)	26 ± 5	9 609	···	>0.10	
1379.60(20)	436	943.97(12)	100	9 442	−21(9)	0.37(8)	1.0 ± 0.4
1799.90(22)	0	1799.73(22)	93 ± 2	70 845	−32(1)	0.10(4)	$2.5^{+2.0}_{-0.8}$
	1216	584.43(10)	6 ± 2	4 316	−3(5)	···	
	1380	420.86(19)	1 ± 1	557	−8(39)	···	
2132.44(24)	1216	916.44(14)	18 ± 5	16 820	−44(6)	0.48(8)	<0.7
	1800	332.54(P)[i]	82 ± 5	(75 718)	−19(4)[h]		
2823.46(47)	2132	691.02(40)[i]	100	84 000	−4(2)	>0.56	<0.6
3646.79(51)	2823	823.33(20)	100	62 078	−20(2)	0.89(5)	<0.5
3690.78(66)	2823	867.32(47)	100	11 614	−31(9)	>0.80	<0.4
3841.40(70)	2823	1017.94(P)	100	12 000	···	1.00(20)	<0.5
4277.16(67)	3647	630.37(10)	89 ± 3	34 485	−17(2)	0.83(6)	0.20 ± 0.8
	3841	435.76(20)	11 ± 3	(4 367)	···	···	
4827.69(78)	4277	550.53(40)	100	10 604	−69(7)	>0.85	<0.4
5160.95(68)	4277	883.79(11)	100	23 059	−13(2)	>0.85	<0.4
5575.83(84)	4828	748.14(32)	100	6 875	−10(5)	>0.90	<0.2
6417.1(11)	5161	1256.16(80)	100	13 286	−10(5)	0.97(5)	<0.2
8122.6(20)	5576	2546.8(1.5)	100	2 000	···	1.00(20)	<0.5

[a] Corrected for nuclear recoil. Uncertainties in the least significant figure are in parentheses.

[b] An entry of P for the uncertainty indicates that the energy was not measured and the quoted E_γ is determined by the level separations.

[c] The numbers in parentheses are from the literature (Ref. 7).

[d] The relative γ-ray intensity. Values in parentheses are estimated.

[e] The γ-ray angular distribution is given by $W(\theta) = I_\gamma[1 + A_2 P_2(\cos\theta) + A_4 P_4(\cos\theta)]$. The A_4 coefficients were not determined with sufficient accuracy to distinguish them from zero.

[f] The DSAM attenuation factor defined in the text.

[g] The mean life of the level (E_i) extracted from $F(\tau)$.

[h] From Ref. 7.

[i] Unresolved in singles spectra from γ rays assigned to ^{59}Co. The data were obtained from the coincidence data and by using the ^{48}Ca(^{14}N, $3n$)^{59}Co reaction since ^{60}Co is formed very weakly via ^{14}N + ^{48}Ca.

level would then have $J^\pi = 2^+ - 5^+$. It appears likely that the level presently observed at 1216 keV is the other member of this doublet.

The spin-parity assignments for the levels with $E_x > 1300$ keV follow from the arguments outlined in I based on the relative direct feeding, angular distributions, and mean lives. Levels have been observed[12,13] in the ^{59}Co(d, p)^{60}Co and ^{62}Ni(d, α)^{60}Co reactions at 1376, 1799, 2131 keV (± 6 keV) and 1380, 2131 keV (± 10 keV), respectively. The 1376-keV (d, p) level was assigned $l = (1 + 3)$, i.e., $J^\pi = (2^+ - 5^+)$ and the 1380-keV (d, α) level was assigned $L = 3$, i.e., $J^\pi = 2^-$, 3^-, or 4^-. It is not clear whether the presently observed $J = (6)$ 1380-keV level corresponds to either of these states. It seems probable, however, that there is at least a doublet near 1380 keV. The 1799-keV level seen in ^{59}Co(d, p)^{60}Co is a doublet, the more intense partner of which is assigned $l = 3$, i.e., $J^\pi = 0^+ - 7^+$. This is consistent with our $J = (6)$ assignment to the 1800-keV level, and we tentatively assume that these (^{15}N, $3n$) and (d, p) observations pertain to the same level. Both the (d, p) and (d, α) angular distribution results for the 2131-keV level are uncertain. The (d, p) results are more reliable because of the more distinctive angular distributions

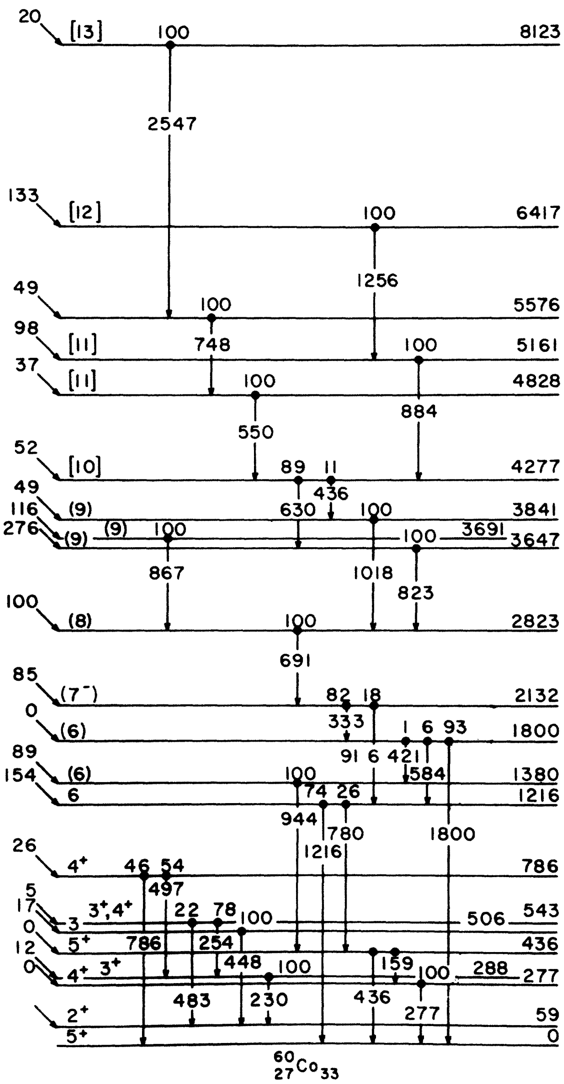

FIG. 9. Level scheme for ^{60}Co deduced from observation of γ rays in the ^{48}Ca(^{15}N, $3n$)^{60}Co reaction. The notation is similar to that of Figs. 1, 6, and 8. Data on the γ-ray transitions are given in Table VI.

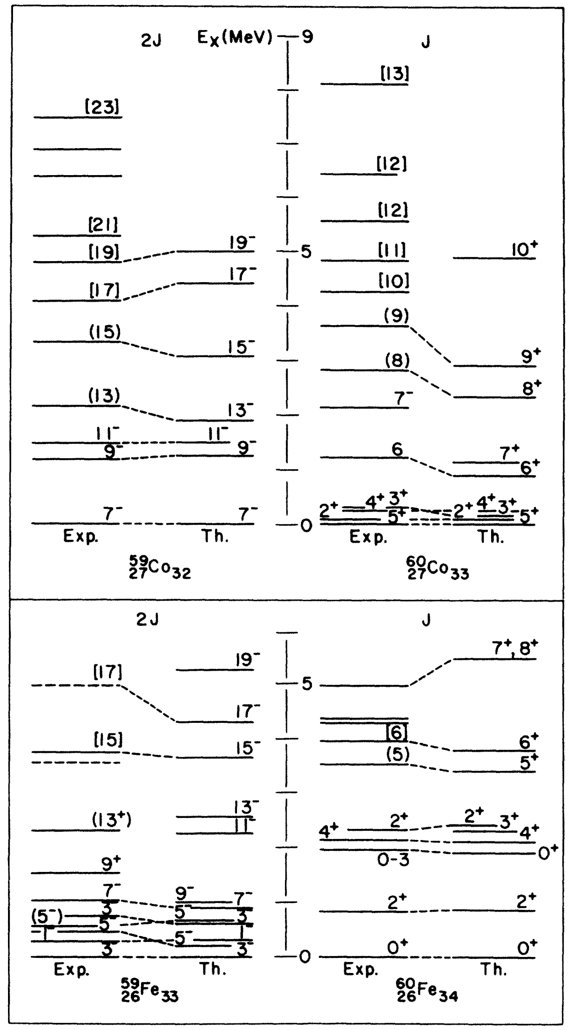

FIG. 10. Comparison of experimental observations and theoretical predictions for yrast states (or near-yrast states) for the nuclei studied in the present investigation. Correspondences are indicated by dashed lines. The theoretical spectra were calculated with the ORNL-Rochester shell-model computer code, and assumes a closed ^{48}Ca core ($N=28$, $Z=20$). The experimental spectra are based on the data presented and reviewed in this survey.

observed for this reaction, and the corresponding $l=(4)$ assignment would allow $J^{\pi}=0^{-}-8^{-}$. We tentatively choose odd parity for the 2132-keV level on the basis of this measurement. Finally, we note that previous work has not disclosed any levels which can be set forth as candidates for association with the levels we observe for $E_x > 2500$ keV (see Fig. 9).

As was the case for ^{59}Co, most of the γ transitions depopulating ^{60}Co levels with $E_x > 1$ MeV exhibited Doppler shifts. No transitions were observed in the ^{15}N + ^{48}Ca RDM measurements which had mean lives long enough ($\tau \gtrsim 6$ ps) to be measured, so that the mean lives listed in Table VI were all deduced from the DSAM.

III. DISCUSSION

The shell-model calculations described in I included results for ^{59,60}Fe and ^{59,60}Co. In these calculations, carried out with the Oak Ridge-Rochester shell-model computer program,[14] the configurational space considered was

$$[\pi(1f_{7/2})^{-n} \otimes \nu(2p_{3/2}, 1f_{5/2}, 2p_{1/2})^{m}], \qquad (2)$$

where $n=28-Z$ and $m=N-28$. The results of this shell-model calculation are compared with the available experimental data on yrast states in ^{59,60}Fe and ^{59,60}Co in Fig. 10. Except for a few low-lying levels, only the predicted yrast levels are shown. A similar comparison was made in I for $A = 52-56$ nuclei, which disclosed an excellent one-to-one correlation between observed and predicted yrast levels. Inspection of Fig. 10 indicates that this is not the case for $A = 59, 60$. Not only do some of the yrast states in ^{59}Fe and ^{60}Co appear to have the wrong parity to belong to the configurational space of (2), but the observed levels appear to have values of J greater than can be generated from (2). Thus there is evidence in $A = 59, 60$ for configurations which could be generated by promoting one or more nucleons out of the $1f_{7/2}$ shell into the $(2p_{3/2}, 1f_{5/2}, 2p_{1/2})$ shell, and neutrons from the $(2p_{3/2}, 1f_{5/2}, 2p_{1/2})$ shell into the $g_{9/2}$ shell. We now consider some specific points of interest for the four nuclei in turn.

A. ^{59}Fe

The comparison shown includes all six of the lowest-lying levels in order to illustrate that a $J^\pi = \frac{5}{2}^-$ assignment to the 571-keV level is in agreement with predictions, whereas the assignment $J^\pi = \frac{3}{2}^-$ previously suggested is not. A candidate for the yrast $J^\pi = \frac{9}{2}^-$ level was not observed, suggesting that the lowest-lying $\frac{9}{2}^-$ level probably appears above the $\frac{9}{2}^+$ level. However, this suggestion involves a minor discrepancy since the yrast $\frac{9}{2}^-$ level is in fact predicted to be at considerably lower excitation. In contrast, the nonappearance of yrast $\frac{11}{2}^-$ and $\frac{13}{2}^-$ levels is satisfactorily explained by the observation that the $\frac{13}{2}^+$ level lies at lower excitations than either of these states.

The 494-keV 1517 → 1023 transition is identified as an $E1\,\frac{9}{2}^+ \to \frac{7}{2}^-$ decay with a strength of $(2.5 \pm 0.7) \times 10^{-5}$ W.u. The large retardation is not surprising for a deexcitation predominantly of the type

$$\nu(2p_{3/2}, 1f_{5/2}, 2p_{1/2})^{m-1}\,\nu g_{9/2} \to \nu(2p_{3/2}, 1f_{5/2}, 2p_{1/2})^{m} \tag{3}$$

since an $E1$ transition is in this case clearly j forbidden. Conversely, the $(\frac{13}{2}^+) \to \frac{9}{2}^+$ $E2$ transition between the 2312- and 1517-keV levels has a comparatively large quadrupole strength of 27 ± 3 W.u. This would be in accord with expectations for a transition between two states generated by the weak coupling of a $g_{9/2}$ neutron to the 0_1^+ and 2_1^+ levels of ^{58}Fe. In ^{58}Fe the 2_1^+ level lies at 811 keV and the strength of the $E2$ 811 → 0 decay is 14.6 ± 2.9 W.u.[15] The greater strength of the corresponding ^{59}Fe transition would then suggest that the $g_{9/2}$ neutron polarizes the ^{58}Fe core to a considerable extent. In this picture of ^{59}Fe, the next yrast level would lie at ~3577 keV, as based on the 4^+-2^+ separation in ^{58}Fe of 1265 keV. Further study of the ^{59}Fe even-parity yrast levels would thus appear to be of some interest.

B. ^{60}Fe

As is evident from Fig. 10, the theoretical predictions for the 0_1^+-2_1^+-4_1^+ states are in excellent accord with the experimental findings derived from the (t,p) and heavy-ion studies. A reasonable correspondence is also evident for the higher-spin states observed in the heavy-ion studies, although again one would like to obtain confirming evidence on those states suggested as 5^+ and 6^+, as well as on the highest-lying states for which no definitive information is presently available. As noted previously, the 1291-keV $4^+ \to 2^+$ and 824-keV $2^+ \to 0^+$ $E2$ transitions are enhanced, with measured strengths of 13.3 ± 3.0 and 13.0 ± 2.0 W. u., respectively.

Also included in Fig. 10 are the 0_2^+ and 2_2^+ states observed in the (t,p) reaction, for which the theoretical predictions of (2) give very good agreement. The 3_1^+ state was not observed in either of the two heavy-ion reactions, and in view of its placement *above* the 4^+ yrast state, this is not surprising. On the other hand, the (t,p) reaction is expected to populate predominantly natural-parity states, even at 3.5-MeV bombarding energy, and thus it is quite likely that the cross section for formation of the 3_1^+ state is too small to permit its observation in the ^{58}Fe$(t,p)^{60}$Fe reaction.

The information derived thus far on the level structure of this $T_z = 4$ even-even nucleus is sufficiently interesting to warrant further study. A recent investigation by Davids and colleagues of the (t,p) reaction at higher triton bombarding energies can be expected to disclose more detailed information on higher-excited states of spin up to 4 or 5. Subsequent investigation of the γ decay of these states via the ^{58}Fe$(t,p\gamma)^{60}$Fe reaction would also be worthwhile. Information on higher-lying yrast states, together with substantiating data on those displayed in Fig. 10, would best be obtained via heavy-ion reactions. The ^{48}Ca$(^{18}$O$, 2n\alpha)^{60}$Fe and ^{48}Ca$(^{15}$N$, p2n)^{60}$Fe reactions were selected for the present study, with the ^{18}O and ^{15}N bombarding energies adjusted to correspond to the peak in the three-nucleon evaporation cross section in order to obtain a maximum probability for formation of ^{60}Fe. Even under these circumstances, the cross section is relatively small because the evaporation process from the highly neutron-rich compound nucleus (^{66}Ni or ^{63}Co) strongly favors sequential emission of neutrons, as opposed to either alphas or protons; i.e., the deexcitation process follows the most direct route back to the valley of stability. Unfortunately, the conclusion therefore is that the two reactions utilized are indeed the most favorable for study of ^{60}Fe. The only obvious improvements therefore would be (1) to use a slightly higher bombarding energy to promote more favorable population of higher-lying states, (2) to increase the experimental running time to improve the counting statistics, or (3) to observe γ rays in coincidence with protons or α particles in order to enhance the channel leading to ^{60}Fe.

C. ^{59}Co

The correspondence between the probable experimental yrast spectrum and the predictions shown in Fig. 10 is satisfactory up to $J=\frac{19}{2}$, although we cannot say the experimental levels do in fact have odd parity. The configurational space of (2) does not produce states with $J>\frac{19}{2}$. Thus, the $J=\frac{21}{2}$ and $\frac{23}{2}$ states of Figs. 8 and 10 are presumably from particle-hole excitations of (2). Whether they have even or odd parity is then of some interest.

D. ^{60}Co

Here the nonappearance of a candidate for the $J^\pi=7^+$ yrast state is a minor discrepancy. Odd-parity states from $g_{9/2}$ excitations out of the configurational space of (2) appear to begin at about 2-MeV excitation, obscuring any correlation between experiment and the predictions of (2) for $J\geq 7$. Again as in ^{59}Co, the observed yrast spectrum extends to higher spins ($J>10$) than allowed in the configurational space considered.

We would like to thank Dr. C. N. Davids for communication of the ^{58}Fe$(t,p)^{60}$Fe results prior to publication.

†Work performed under the auspices of the U.S. Energy Research and Development Administration.

*Research sponsored by the U.S. Energy Research and Development Administration under contract with Union Carbide Corporation.

[1]A. M. Nathan, J. W. Olness, and E. K. Warburton, Phys. Rev. C 16, 192 (1977).

[2]H. J. Kim, Nucl. Data Sheets 17, 485 (1976).

[3]K. C. McLean, S. M. Polgliesh, S. S. Ipson, and G. Brown, Nucl. Phys. A191, 417 (1972); A. Sperduto and W. W. Buechner, Phys. Rev. 134, B142 (1964).

[4]R. C. Pardo, C. N. Davids, M. J. Murphy, E. B. Norman, and L. A. Parks, Phys. Rev. C 16, 370 (1977).

[5]H. J. Rose and D. M. Brink, Rev. Mod. Phys. 39, 306 (1967).

[6]J. J. Kolata, J. W. Olness, and E. K. Warburton, Bull. Am. Phys. Soc. 18, 653 (1973).

[7]H. J. Kim, Nucl. Data Sheets 16, 317 (1975).

[8]A. E. Litherland and A. J. Ferguson, Can. J. Phys. 39, 788 (1961).

[9]A. R. Poletti and E. K. Warburton, Phys. Rev. 137, B595 (1965).

[10]P. M. Endt and C. van der Leun, At. Data Nucl. Data Tables 13, 1 (1974).

[11]J. F. Mateja, A. Bieszk, J. T. Meek, J. D. Goss, A. A. Rollefson, P. L. Jolivette, and C. P. Browne, Phys. Rev. C 13, 2269 (1976).

[12]H. A. Enge, D. L. Jarrell, and C. C. Angelman, Phys. Rev. 119, 735 (1960).

[13]W. Seliger, D. Bachner, H. Kelleter, and B. Schmidt, Nucl. Phys. A184, 599 (1972).

[14]J. B. French, E. C. Halbert, J. B. McGrory, and S. S. M. Wong, in *Advances in Nuclear Physics*, edited by M. Baranger and E. Vogt (Plenum, New York, 1969), Vol. 3.

[15]A. M. Nathan, J. W. Olness, and E. K. Warburton (unpublished), planned as the third paper in this series.